In vivo NAD assay reveals the intracellular NAD contents and redox state in healthy human brain and their age dependences

Xiao-Hong Zhu[1], Ming Lu, Byeong-Yeul Lee, Kamil Ugurbil, and Wei Chen[1]

Center for Magnetic Resonance Research, Department of Radiology, University of Minnesota Medical School, Minneapolis, MN 55455

Edited by Marcus E. Raichle, Washington University in St. Louis, St. Louis, MO, and approved January 27, 2015 (received for review September 16, 2014)

NAD is an essential metabolite that exists in NAD^+ or NADH form in all living cells. Despite its critical roles in regulating mitochondrial energy production through the NAD^+/NADH redox state and modulating cellular signaling processes through the activity of the NAD^+-dependent enzymes, the method for quantifying intracellular NAD contents and redox state is limited to a few in vitro or ex vivo assays, which are not suitable for studying a living brain or organ. Here, we present a magnetic resonance (MR) -based in vivo NAD assay that uses the high-field MR scanner and is capable of noninvasively assessing NAD^+ and NADH contents and the NAD^+/NADH redox state in intact human brain. The results of this study provide the first insight, to our knowledge, into the cellular NAD concentrations and redox state in the brains of healthy volunteers. Furthermore, an age-dependent increase of intracellular NADH and age-dependent reductions in NAD^+, total NAD contents, and NAD^+/NADH redox potential of the healthy human brain were revealed in this study. The overall findings not only provide direct evidence of declined mitochondrial functions and altered NAD homeostasis that accompany the normal aging process but also, elucidate the merits and potentials of this new NAD assay for noninvasively studying the intracellular NAD metabolism and redox state in normal and diseased human brain or other organs in situ.

redox state | NAD | in vivo ^{31}P MR spectroscopy | human brain | aging

NAD, a multifunctional metabolite found in all living cells, has been the interest of many scientific investigations since its discovery in the early 20th century (1). NAD is known to convert between its oxidized NAD^+ and reduced NADH forms during the breakdown of nutrients; hence, the intracellular NAD^+/NADH redox state reflects the metabolic balance of the cell in generating ATP energy through oxidative phosphorylation in mitochondria and/or glycolysis in cytosol (2). More recently, after several protein families associated with cell survival were found to use NAD^+ as their main substrate with activities also regulated by the availability of the NAD^+, the full extent of the NAD's function as a metabolic regulator began to unfold (3–5). A growing number of studies have indicated that NAD^+ can modulate metabolic signaling pathways and mediate important cellular processes, including calcium homeostasis, gene expression, aging, degeneration, and cell death; therefore, the cellular NAD could serve as a therapeutic target for treating various metabolic or age-related diseases and promoting longevity (6–12).

Despite the critical relevance of the intracellular NAD metabolism to human health and diseases, assessment of NAD contents and NAD^+/NADH redox state is extremely challenging. Only a few invasive techniques based on biochemical assays or autofluorescence methods have been used to analyze tissue samples or cell extracts (13, 14). However, during the preparation of such ex vivo sample, the NAD^+ and NADH contents are likely altered, because they are highly sensitive to pH, temperature, light, and chemical agent or buffer solution. Thus, accurate quantification and extrapolation to in vivo conditions are difficult, even with the well-established biochemical assays (15). In addition, NAD^+ does not fluoresce and thus, cannot be detected by fluorometry (16). Clearly, a nondestructive detection and quantification method is highly desired to investigate the NAD contents and redox state in the human body or intact animal models.

Recently, we have developed a novel magnetic resonance (MR) -based quantification approach that uses a high-field MR scanner to obtain the endogenous ^{31}P MR signals of the NAD molecules in intact animal brains (17). Distinct from earlier ^{31}P MR spectroscopy (MRS) studies that reported total NAD contents (18–20), our approach is able to resolve the MR signal of NADH from that of NAD^+ by taking advantage of their specific spectroscopic characteristics at a given magnetic field strength that can be precisely predicted based on a theoretical model (17). Thus, both NAD^+ and NADH can be quantified simultaneously by matching the in vivo NAD spectra with the model-simulated spectra. It has been shown that this approach works well in animal brains at ultrahigh fields of 9.4 and 16.4 T (17). In this study, we further exploit the feasibility and potential of this novel approach for noninvasive assessment of intracellular NAD^+ and NADH contents and NAD^+/NADH redox state in healthy human brains using a 7-T human MR scanner and ultimately, studying their roles in human aging.

Results

In Vivo ^{31}P MRS of Human Brain at 7 T. Fig. 1 displays the in vivo ^{31}P MR spectra acquired from the occipital lobes in two representative healthy subjects with different ages. In addition to the commonly observed phosphorus metabolites, such as phosphocreatine (PCr), ATP (γ-, α-, and β-ATP), P_i, phosphomonoester,

Significance

Decline in NAD^+ availability and abnormal NAD^+/NADH redox state are tightly linked to age-related metabolic diseases and neurodegenerative disorders. To better understand the roles of NAD metabolism and redox state in health and disease, it is important to assess the intracellular NAD and redox state in situ. We report herein the first in vivo NAD assay, to our knowledge, that is capable of noninvasively and simultaneously measuring intracellular NAD^+ and NADH concentrations and NAD^+/NADH ratio in the human brain and detecting the age-dependent changes in NAD contents and redox state associated with the normal aging. This method can potentially be applied to study various metabolic and neurodegenerative disorders by monitoring the NAD and redox state changes associated with disease progression or treatment in human patients.

Author contributions: X.-H.Z. and W.C. designed research; X.-H.Z. and B.-Y.L. performed research; M.L. and W.C. contributed new reagents/analytic tools; X.-H.Z. and M.L. analyzed data; X.-H.Z., K.U., and W.C. wrote the paper.

The authors declare no conflict of interest.

This article is a PNAS Direct Submission.

[1]To whom correspondence may be addressed. Email: zhu@cmrr.umn.edu or wei@cmrr.umn.edu.

This article contains supporting information online at www.pnas.org/lookup/suppl/doi:10.1073/pnas.1417921112/-/DCSupplemental.

www.pnas.org/cgi/doi/10.1073/pnas.1417921112

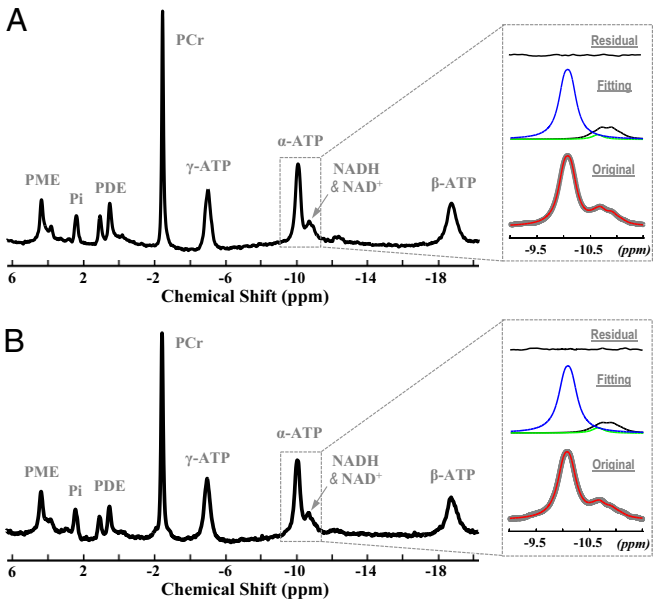

Fig. 1. In vivo ^{31}P MR spectra of two representative subjects at ages (*A*) 36 and (*B*) 52 y old. They were obtained within 16 min from human occipital lobe, where the ^{31}P coil (5 cm in diameter) sensitivity profile was verified by in vivo ^{31}P chemical shift imaging in a previous study (19). *Insets* display the expanded spectra in the chemical shift range from −9.0 to −11.5 ppm with the original in vivo ^{31}P signals (gray) and the total signals (red) of α-ATP and NAD determined by the model fitting. The individual fitting components of α-ATP (blue), NAD^+ (black), and NADH (green) and the residual signal of the fitting are also shown. The quantification results of NAD^+/NADH ratio (RX) of (*A*) 4.8 and (*B*) 3.4 indicate a lower redox state for the older subject. PDE, phosphodiester; PME, phosphomonoester.

and phosphodiester, the resonances on the right-side shoulder of the α-ATP were identified as NAD^+ and NADH. These spectra represent the high-quality in vivo ^{31}P MRS data obtainable from the human brain at 7 T with a relatively short acquisition time of 16 min. In particular, the excellent signal-to-noise ratio (SNR) of the ^{31}P spectra ($SNR_{PCr} = 216 \pm 24$ and $SNR_{\alpha\text{-ATP}} = 91 \pm 7$; $n = 11$) ensured reliable spectral fitting and NAD quantification. Although it is difficult to determine the actual SNRs of NAD and NADH because of their complex spectral patterns and signal overlapping, we were able to measure the SNR of 17 ± 2 ($n = 11$) for the right-side apparent NAD doublet, which is mainly attributed to the NAD^+ signal, and the SNR of 23 ± 2 ($n = 11$) for the left-side apparent NAD doublet, which are the superimposed NAD^+ and NADH signals, respectively.

NAD Quantification in Human Brain at 7 T. Fig. 1 *A*, *Inset* and *B*, *Inset* displays the experimentally measured (Fig. 1, gray traces) and model-fitted (Fig. 1, red traces) spectra within the chemical shift range that contain the NAD^+, NADH, and α-ATP resonances. The NAD quantification was done by the least-square fitting of the in vivo NAD spectra to the NAD model simulation at the field strength of 7 T. The individual spectrum of NAD^+ (a quartet with different chemical shifts and peak ratios that are field-dependent) and NADH (a singlet with a field-independent chemical shift) as well as their combined resonance signals at 7 T with different resonance linewidths (LWs; e.g., LW = 8, 16, and 24 Hz) and a typical NAD^+/NADH ratio of four were exemplified in Fig. S1. Fig. S1 illustrates how the NAD spectra evolve with increasing resonance LWs, which mimics the sample conditions from an ex vivo solution toward in vivo tissue. Therefore, in an intact brain, the five sharp peaks that characterize the spectrum of NAD^+ and NADH mixture merge into an apparent doublet shown in Fig. 2, which also includes the α-ATP resonance in the combined spectra. Fig. 2*A* displays the simulated individual spectra of NAD^+ and NADH or combined spectra of NADH plus NAD^+ and α-ATP plus NADs. The corresponding spectra are shown in Fig. 2*B*, which displays the in vivo spectrum of a human brain (Fig. 2*B*, row 1) and the decomposition to its individual components. Strikingly, the real and simulated spectra are almost identical, except for the noise contained in the in vivo data. This result is consistent with the small fitting residues seen in Fig. 1 *A*, *Inset* and *B*, *Inset* and suggests that the NAD quantification method is capable of differentiating the NAD^+ and NADH signals detected by in vivo ^{31}P MRS in the human brain.

By using the α-ATP resonance signal as an internal standard and assuming [ATP] = 2.8 mM in the normal brain tissue (17, 21, 22), we were able to noninvasively obtain quantitative data for the human brain on 17 healthy subjects spanning the ages of 21–68 y old. The results yielded the following intracellular concentrations: $[NAD^+] = 0.30 \pm 0.02$ mM or 0.27 ± 0.02 μmol/g (after a unit conversion using a brain tissue density of 1.1 g wet brain tissue per 1 mL), $[NADH] = 0.06 \pm 0.01$ mM or 0.06 ± 0.01 μmol/g, and total NAD ($[NAD]_{total} = [NAD^+] + [NADH]$) = 0.37 ± 0.02 mM or 0.34 ± 0.02 μmol/g. Consequently, the intracellular NAD^+/NADH redox ratio (RX; $RX = [NAD^+]/[NADH]$) and redox potential (RP) were calculated to be 4.8 ± 0.9 and -299.3 ± 2.5 mV, respectively.

Reproducibility and Reliability of the in Vivo NAD Assay. To evaluate the reproducibility of the MR-based in vivo NAD assay, we performed repeated measurements in the same subject either within the same scan session or on two different days. The results are summarized in Fig. S2. The fact that all of the data points are at or near the identity line between the first and second measurements indicates high reproducibility of the assay. This finding is also consistent with the small test–retest coefficient of variance (CV)

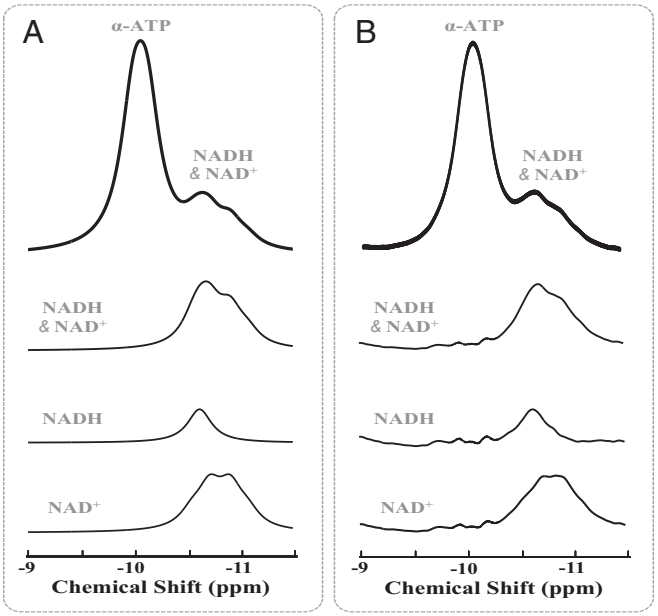

Fig. 2. Simulated and in vivo ^{31}P MR spectra of the human brain at 7 T. (*A*) Model-simulated spectra of NAD^+ quartet, NADH singlet, total NAD, and combined α-ATP and NAD signals with an HLW of 18 Hz and an NAD^+/NADH RX of 3.35. (*B*) Experimentally measured in vivo ^{31}P MR spectra of human occipital lobe processed with 10-Hz line broadening that have the same HLW and RX values as the simulated spectra in *A*. The individual and combined in vivo spectra of NAD^+, NADH, and total NAD were obtained by subtracting corresponding fitting components from the original brain spectra.

NEUROSCIENCE

defined as the ratio of the SD and the mean calculated for [NAD^+] (CV = 2.4%, n = 7), [NADH] (CV = 6.0%, n = 7), $[NAD]_{total}$ (CV = 2.3%, n = 7), and RX (CV = 5.1%, n = 7) in the human brain.

The reliability of the assay was also estimated through model simulation to determine the accuracy and errors of the NAD quantification when different levels of random noise were added to a sample NAD spectrum with known NAD contents, RX, and resonance one-half LW (HLW). The results are summarized in Table S1, in which several $SNR_{\alpha\text{-}ATP}$ values ($SNR_{\alpha\text{-}ATP}$ = 20, 40, 60, 80, and 100) were used for the simulation. In general, we found that accurate quantification (with fitting accuracy of ≤1%) and small error (fitting error of ≤5%) can be achieved when $SNR_{\alpha\text{-}ATP}$ is 40–60 or higher. Considering the superior spectral quality and excellent SNR of the ^{31}P MRS data presented in this study (i.e., $SNR_{\alpha\text{-}ATP}$ > 90), the in vivo NAD assay for human brain application at 7 T should be highly reliable and sensitive to brain physiology and pathology changes.

Age-Dependent Changes of NAD Contents and Redox State in Healthy Human Brain. When carefully examining the ^{31}P MR spectra of various subjects, we noticed a small but visible difference in the NAD signals, indicating a different peak ratio of the apparent NAD doublet in older volunteers compared with their younger counterparts (example in Fig. 1). To verify this interesting observation, the concentrations of the NAD^+, NADH, and total NAD and the NAD^+/NADH RP of each subject were plotted against his/her age. This plot (Fig. 3), indeed, shows the existence of age-dependent changes in all of the above measures. The individual data (Fig. 3, open symbols) showed a positive age correlation for [NADH] (Pearson's correlation coefficient r = 0.68) and negative age correlations for [NAD^+] (r = −0.75), $[NAD]_{total}$ (r = −0.57), and RP (r = −0.76). When the in vivo ^{31}P MR spectra of individual subjects were averaged within three age groups (Fig. 3, filled symbols) and reanalyzed, excellent linear correlations to age (the square of linear regression coefficient: $R^2 \geq$ 0.99) were found for [NAD^+], [NADH], $[NAD]_{total}$ (Fig. 3*A*), and the NAD^+/NADH RP (Fig. 3*B*), whereas the NAD^+/NADH RX had a strong age dependence slightly off from a linear function.

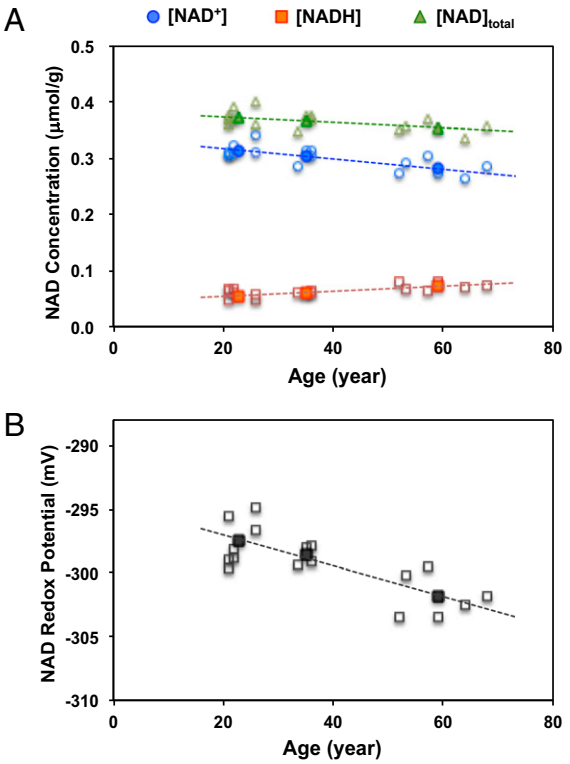

Fig. 3. Age dependences of (*A*) intracellular NAD^+, NADH, and total NAD concentrations and (*B*) NAD^+/NADH RP observed in healthy human brains. The open symbols represent individual subject data, and the filled symbols display the average data from three age groups of younger (21–26 y old; n = 7), middle (33–36 y old; n = 4), and older (59–68 y old; n = 6) subjects.

Discussion

Methodology Aspects of the MR-Based in Vivo NAD Assay. In this study, we showed the feasibility of spectral decomposition of ultrahigh-field (7 T) ^{31}P MRS as an in vivo NAD assay for noninvasively determining the cellular NAD^+, NADH, and total NAD concentrations as well as the NAD^+/NADH redox state in the healthy human brain. All of this information is collected simultaneously with one relatively short MR measurement. The reliability and reproducibility of this assay have been rigorously evaluated in this study, and the results indicate that highly reliable and reproducible measurements are obtainable in the human brain at 7 T. To ensure accurate determination of the low-concentration NAD metabolites and the NAD^+/NADH redox state, several critical issues that relate to the methodology of this assay are discussed below.

First, a high-quality ^{31}P MR spectrum, as shown in Fig. 1, particularly with high SNR and narrow resonance LW, is necessary for the success of the assay. Although LWs in hertz units increase with increasing magnetic field strength, the spectral resolution that is determined by the resonance LW in parts per million units improves substantially at higher fields (23). In this regard, a high-/ultrahigh-field MR scanner is advantageous because of the sensitivity gain and the spectral resolution improvement (23).

Second, knowledge of the specific NAD spectral pattern at a given field of the MR scanner is required for model simulation and spectral fitting of the in vivo ^{31}P MR data. Based on the MR physics, known molecular structures, and chemical shift information of the NAD^+ and NADH, the exact pattern of the NAD spectrum, including the chemical shifts and peak ratios of different NAD^+ resonances at a given field strength, can be precisely predicted (17, 24). With this information, one can fit all of the NAD^+ and NADH resonances together; hence, the statistical power for achieving reliable quantification for the low-concentration metabolites will be much higher than fitting them independently.

Third, most ^{31}P MRS measurements are not performed under fully relaxed conditions to save the scan time and gain SNR per unit of sampling time. Thus, the longitudinal relaxation time (T_1) of the NAD at a given field will be useful for correcting the saturation effect that leads to an underestimation in the metabolite concentration. T_1 values of NAD^+ and NADH have been determined in the cat brain at 9.4 and 16.4 T (17). They were found to be similar to each other at the same field strength and increase at lower field (17, 23). The T_1 values of NADs in human brain at 7 T are not determined yet, but they could be estimated from the known T_1 values of cat brain at 9.4 and 16.4 T, assuming that their field-dependent behaviors are similar as those of α-ATP (17, 23). Therefore, the actual tissue concentrations of [NAD^+], [NADH], and $[NAD]_{total}$ in human brains are estimated to be ∼16% higher than those reported in this study after correcting the saturation effect. The NAD^+/NADH RX and RP, however, do not require such corrections because of the similar T_1 values of NAD^+ and NADH, thus, the same saturation effects at the same field strength (17).

Fourth, biological studies have suggested that NAD^+ and NADH could exist in free or protein-bound forms and can be located and metabolized in different subcellular compartments (e.g., cytosol and mitochondria) (25, 26). However, the MR-based NAD assay is unable to distinguish these differences; it only measures their total contents and their ratio in the tissue, similar to what biochemical assays are supposed to measure,

albeit in ex vivo samples (17). Earlier studies using the metabolite indicator method with the equilibrium assumption of enzymatic reactions had calculated redox state of free NADs in cytoplasm and shown that it can be over 100 times higher than that of mitochondria (27). However, experimental measurements in isolated rat hypatocytes (28) reveal that, although the individual concentrations of NAD^+ and NADH were significantly different in cytosol and mitochondria, the total (free plus bound) NAD^+/NADH ratios in the two compartments were, in fact, in the same magnitude (i.e., ~2.4 in cytosol vs. 9.4 in mitochondrion). Therefore, after considering the variation of the mitochondrial contents and the corresponding compartmental distribution of NADs in different cell types (25, 26), we believe that the in vivo NAD assay measures the mean contributions from both mitochondrial and cytosolic pools. The experimental evidences obtained in animal and human brains as shown in this and previous (table 4 in ref. 17) studies support this notion.

Physiological Implication of the in Vivo NAD Assay Findings. By applying this new MR measurement of NAD, we were able to determine the intracellular NAD^+ and NADH concentrations and the NAD^+/NADH redox state in the brains of healthy volunteers while they were resting inside an MR scanner. To our knowledge, these values in the human brain have never been reported before owing to the lack of appropriate detection methods; they are within the range of the literature values obtained in rodent brains with in vitro or ex vivo methods (ref. 17, references therein and table 4). Therefore, we anticipate that the NAD contents and redox states of human brain as reported herein could provide a valuable reference for future studies aiming to understand the roles of the NAD and NAD^+/NADH redox state and their alterations in healthy and diseased human brains. Consequently, the values of NAD contents and ratios obtained with the in vivo NAD assay could become a new gold standard as long as the concentration of ATP or other quantifiable resonances in the ^{31}P spectrum have been accurately determined and sufficient SNR and appropriate correction for saturation effects are attained.

NAD plays two distinct roles in regulating cellular metabolism and signaling as schematically summarized in Fig. 4. NAD could function as a coenzyme and participate in many important oxidative–reductive reactions of the cellular respiration processes, where the NAD^+/NADH ratio regulates the energy production. In the brain, most NADH molecules are produced (from NAD^+) during the breakdown of glucose through glycolysis (two NADH) in cytosol, pyruvate decarboxylation (two NADH), and the tricarboxylic acid (TCA) cycle (six NADH) in mitochondria. The NADH molecules as the electron donor are converted back to NAD^+ in the mitochondrial electron transport chain, whereas the oxygen (O_2) molecules receive the electron; the energy harvested in this process is used to drive the ATP synthesis (Fig. 4). Therefore, the NADH production is tightly linked to the brain carbohydrate metabolism and reflects the cerebral metabolic rate of glucose (CMR_{glc}). In contrast, the NAD^+ production is linked to the electron transport chain reactions and reflects the cerebral metabolic rate of oxygen (CMR_{O2}). These processes are regulated by the intracellular NAD^+/NADH redox state, which determines the metabolic balance between the cellular carbohydrate and oxygen metabolisms in supporting the brain ATP energy under normal or diseased condition (2, 29, 30). We hypothesize that the intracellular NAD^+/NADH RX could provide a single valuable measure directly linking to the metabolic oxygen-to-glucose index defined by the CMR_{O2}/CMR_{glc} ratio, which is an essential biomarker of the neuroenergetics for various brain states (31).

In this study, we found a gradual but significant decline in the human brain NAD^+/NADH RX (or RP) associated with a decreasing NAD^+ level and an increasing NADH level in the process

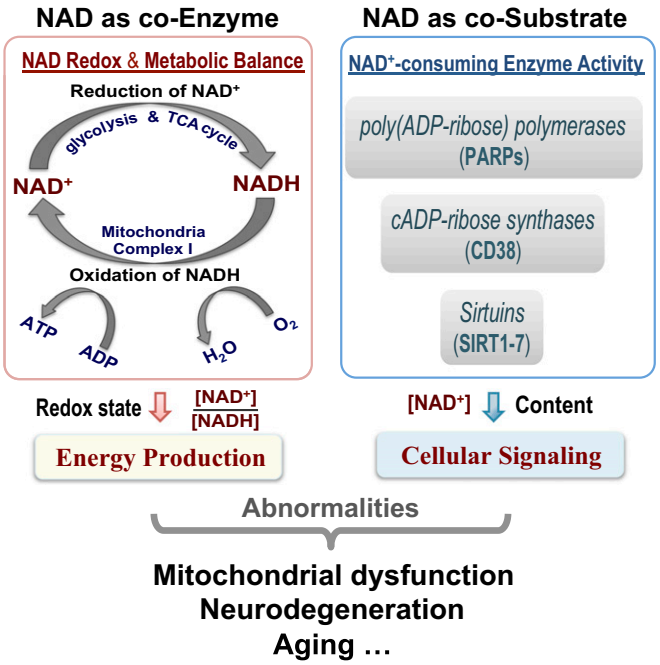

Fig. 4. A simplified scheme summaries the major functions of intracellular NAD: NAD as a coenzyme in regulating the glucose–oxygen metabolic balance that controls the cerebral ATP energy production through the NAD^+/NADH redox state (*Left*), and NAD^+ as a cosubstrate in modulating the activities of the NAD^+-consuming enzymes that mediate the cellular signaling processes through the availability of cellular NAD^+ (*Right*). The abnormality in either one or both of these functions could lead to mitochondrial dysfunction, neurodegeneration, or age-related metabolic disorders.

of healthy aging. Various biological factors could contribute to the slow declines in mitochondrial metabolism efficiency and functionality during aging (32). Among them, the cellular NAD contents and NAD^+/NADH redox state are expected to play crucial roles (33). The strong age dependences of intracellular [NAD^+], [NADH], RX, and RP observed in this study provide the first in vivo evidence, to our knowledge, that connects human aging to the changes in cerebral NAD contents and redox state. This finding is in agreement with ex vivo studies showing the same trends of NAD changes found in rodent brains of different age groups (34, 35).

The decline in brain NAD^+/NADH RX suggests a significant shift of the glucose–oxygen metabolic balance toward slower oxygen metabolism and oxidative phosphorylation in the mitochondria, resulting in a lower ATP production rate in aging brains. Significant CMR_{O2} reduction and relatively constant CMR_{glc} (i.e., a reduced oxygen-to-glucose index) in older people have been reported (36, 37). Moreover, the notion that age-induced decrease in NAD^+/NADH RX reflects deficiency in mitochondrial capacity for oxidative phosphorylation is also supported by significant decreases (e.g., 15–34%) in respiratory enzyme (complexes I–V) activities observed in aged mice brains (38), which is in line with another human brain study showing an ~30% reduction in both neuronal oxidative glucose metabolism and neurotransmission cycling rates in elderly people (39). A similar reduction (~40%) of mitochondrial oxidative and phosphorylation activities was also observed in the human skeletal muscle during healthy aging, suggesting that the decline in mitochondrial functionality should be a global phenomenon in the aging process (40).

In addition to governing energy homeostasis through regulating the NAD^+/NADH redox state, the biosynthesis and catabolism of NAD^+ can influence the activity of various enzymes that mediates metabolic processes in the cell. As shown in Fig. 4, *Right*, NAD^+ could also function as a cosubstrate for several classes

of NAD^+-consuming enzymes, including poly(ADP ribose) polymerases (PARPs), cADP ribose synthases (CD38), and sirtuins (SIRTs; SIRT1–7). These enzymes were found to play important roles in cellular signaling related to cell death, Ca^{2+} homeostasis, and lifespan extension, and their activities are highly dependent on the level of NAD^+ available in the cell (4, 5, 8, 9, 33, 41, 42).

In this study, other than the decreases in the intracellular NAD^+ level and RX (or RP), we also observed a slower decline of the total intracellular NAD content in the human brain during healthy aging, which collectively reflects reduced NAD^+ availability in the aged brain. One additional note is that the actual reduction of the intracellular NAD pool could be even more than what has been shown here if the brain ATP level is not constant, which is presumed in this study, but rather, decreased as people aged. However, this uncertainty should not change the major findings and conclusions of this work, particularly the findings of the significant declines in $[NAD^+]$, $[NAD]_{total}$, and RX or RP during the aging process, because the consideration of potential ATP decline, if existed, could further accelerate the decline trends reported in this work. The trend of [NADH] increase, however, could be slightly slowed down after taking into account declining ATP level. Additional studies are needed to address this question.

Another note is related to the criterion for identifying the normal subjects in this study, which was based on the comprehensive information provided on the consent form to ensure no obvious history of neurological or psychiatric diseases and no drug or prescription medication for any brain disorder. Nevertheless, a thorough medical examination would be helpful, because many chronic and systematic medical conditions could have impact on the brain before clinical symptoms appear. However, we would anticipate better age dependence if such information was available and if subjects with potential medical problems were excluded.

Declined NAD^+ levels were found to accompany higher PARP and CD38 activity and lower ATP level and SIRT1 activity in older mice and significantly reduced lifespan in worms (8). It has been shown that, by supplying NAD^+ precursors or intermediates and/or introducing PARPs or CD38 inhibitor, one could enhance the NAD^+ biosynthesis and/or inhibit its consumption, thus boosting the intracellular NAD^+ level (6, 10, 11, 43). Such interventions are suggested to promote therapeutic effects of lifespan extension and neuroprotection and could potentially be used with other physiological managements, such as calorie restriction, fasting, or exercise, to compensate for the natural decline of brain NAD^+ in normal aging and prevent or treat age-related metabolic disorders (3, 4, 33, 44, 45).

Potential Uses of in Vivo NAD Assay. The potential applications of this NAD assay as a valuable tool for biomedical and clinical research can be expected in several ways. (*i*) Although this study focused on the human occipital lobe, the same approach could be readily extended to image the spatial distribution of intracellular NAD concentrations and NAD^+/NADH redox state across the entire human brain and monitor their longitudinal changes in the brain and beyond (e.g., heart and muscle) without foreseeable obstacles. (*ii*) It allows evaluation of the intracellular NAD contents and redox state in diseased brain or brain regions to compare them with the corresponding normal brain tissues; thus, it will open new frontiers for studying the central roles of cellular NAD metabolism and redox state in human health and neurodegenerative diseases. (*iii*) This in vivo assay would provide a new means to evaluate the efficacy of the disease-modifying treatment or therapeutic intervention through monitoring the changes of the intracellular NAD content and redox state in addition to other phosphorous metabolite information in diseased human brain or other organs.

In summary, this study presents a sensitive MR-based in vivo NAD assay that is capable of noninvasively assessing the intracellular NAD^+, NADH, and total NAD contents and NAD^+/NADH RX and RP in human brains. This technical advancement made it possible to obtain these important parameters in healthy human brains and study their age-dependent changes in situ. The overall findings provide new insights regarding the cellular NAD^+ availability in the brain, the link between the NAD^+/NADH redox state and the cerebral metabolic balance, and their alterations associated with healthy aging. It is expected that this novel NAD assay should be highly valuable in biomedical and/or clinical research fields aiming to study the intracellular NAD availability, the NAD^+/NADH redox state, and their relationships with mitochondrial dysfunction, neurodegeneration, aging, and longevity.

Methods

In Vivo ^{31}P MRS Measurements of Human Brains. Seventeen human volunteers (age: 21–68 y; 10 males and 7 females) participated in this study, with written informed consent approved by the Institutional Review Board of the University of Minnesota. All of them were healthy and had no history of neurological or psychiatric diseases. Seven of these subjects (four males and three females) were scanned two times either in the same session or on two different days with the same study protocol.

^{1}H MRI and ^{31}P MRS measurements were conducted at 7 T with a 90-cm bore actively shielded human magnet paired with Siemens electronics and gradients using a radiofrequency (RF) probe placed underneath the human occipital lobe for data acquisition. This RF probe consisted of a butterfly-shaped ^{1}H coil for anatomic imaging and B_0 shimming and a single-loop ^{31}P coil (diameter of 5 cm) for collecting in vivo ^{31}P MRS data. The ^{31}P spectra were obtained from the human occipital lobes using the single-pulse acquire sequence with a 300-μs hard excitation pulse, a 3-s repetition time, and a total scan number of 320 for signal averaging. The RF coil position and RF pulse flip angle were optimized to ensure that the detected in vivo ^{31}P MRS signals were mainly attributed from the human occipital lobe (19). The raw free induced decays of the ^{31}P MR data were zero-filled, and a line broadening of 5 or 10 Hz was applied before fast Fourier transformation for enhancing the SNR. The SNR of the ^{31}P MR spectra (line broadening = 5 Hz) was evaluated using the PCr and α-ATP signals and calculated by dividing the resonance height by the peak-to-peak spectral noise and then multiplying it by 2.5 (23). The in vivo ^{31}P MR spectrum of each subject (or for each measurement) was generated, and various phosphorous metabolites were assigned based on their chemical shifts (δ) with that of PCr resonance set at −2.5 ppm as the reference. The spectrum within the chemical shift range of −9 to −11.5 ppm that contains α-ATP, NAD^+, and NADH resonances was phased and baseline-drift corrected to ensure a symmetric α-ATP peak and flat spectral baseline before the NAD quantification was performed.

NAD Quantification and Spectral Model Simulation. The ^{31}P MR spectra of NAD at 7 T can be characterized as follows: NADH is a single resonance (with $\delta_{NADH} = -10.63$ ppm), and α-ATP is a doublet (centered at $\delta_{\alpha\text{-}ATP} = -10.07$ ppm with a J-coupling constant of 15.5 Hz), whereas the NAD^+ has four resonances (i.e., quartet). The chemical shifts and relative peak intensity ratios among these NAD^+ peaks at 7 T were determined based on the second-order coupling effect and calculated from their known values obtained at 11.7 T (details in figure 1 in ref. 17). This information was applied to the NAD quantification model incorporated with a Matlab-based program for simulating and/or fitting the spectra of α-ATP, NAD^+, and NADH resonances through linear summation and regression of the multiple resonances convoluted with Lorentzian line shape function in the frequency domain (17). It was also assumed in the model that the HLWs of the NADH and NAD^+ resonances were the same, but that of α-ATP was slightly (~1.5 Hz) larger, resulting in the best-fitting data.

The outcomes from the regression between the in vivo ^{31}P spectrum and the NAD quantification model prediction gave the signal integrals of NAD^+ and NADH resonances, respectively. The integrals were compared with those of α-ATP, in which its brain concentration was set to 2.8 mM (17, 21); thus, the concentrations of intracellular NADH and NAD^+ in each brain were determined, and the NAD^+/NADH RX and total intracellular NAD concentration ($[NAD]_{total} = [NAD^+] + [NADH]$) were calculated. The NAD^+/NADH RP can be calculated using the Nernst Equation (46, 47):

$$RP = RP^0 + \frac{RT}{zF}\ln\left(\frac{[NAD^+]}{[NADH]}\right) = RP^0 + \frac{RT}{zF}\ln(RX), \quad [1]$$

where RP^0 (–0.32 V) is the midpoint potential of the NAD^+/NADH redox pair, R is the universal gas constant, T is the absolute temperature, F is the Faraday constant, and z is the number of moles of electrons transferred in the redox reaction (2 for the NAD^+/NADH redox reaction). Hence, at the brain temperature of 37 °C,

$$RP = -0.32 + 0.0308\log_{10}(RX)(\text{volt}). \quad [2]$$

To evaluate the reliability of the NAD quantification method and its dependence on the $SNR_{\alpha\text{-}ATP}$ in a ^{31}P MR spectrum, five different levels of randomly generated white Gaussian noise were added to the simulated 7-T ^{31}P spectra with predetermined HLW and NAD^+/NADH ratio values. Monte Carlo simulations with 100 trials for each noise level were performed. The values of the parameters used in the spectral simulation were similar to those of human brains measured in this study: RX = 3.45, [NAD^+] = 0.312 μmol/g brain tissue, [NADH] = 0.090 μmol/g brain tissue, and HLW = 17.5 Hz. By fitting the ^{31}P spectra with different noise (i.e., $SNR_{\alpha\text{-}ATP}$ = 20, 40, 60, 80, and 100), the model-determined values were compared with their true values to estimate the fitting accuracy and error (thus, the reliability of the NAD quantification). The accuracy of the model quantification was defined as accuracy (%) = 100 × abs(mean-real)/real, where real is the predetermined parameter value without added noise. The fitting error was defined as error (%) = 100 × SD/mean for the evaluated parameters.

All results are presented as means ± SDs in the study. The statistical analyses of linear regression reported the regression coefficient (*R*) and Pearson's correlation coefficient (*r*).

ACKNOWLEDGMENTS. This work was supported by NIH Grants RO1 NS041262, NS057560, and NS070839, R24 MH106049, S10 RR026783, P41 EB015894, and P30 NS076408 and the Keck Foundation.

1. Harden A, Young WJ (1906) The alcoholic ferment of yeast-juice. *Proc R Soc Lond B Biol Sci* 77(519):405–420.
2. Chance B, Ito T (1962) Control of endogenous adenosine triphosphatase activity by energy-linked pyridine nucleotide reduction in mitochondria. *Nature* 195:150–153.
3. Belenky P, Bogan KL, Brenner C (2007) NAD^+ metabolism in health and disease. *Trends Biochem Sci* 32(1):12–19.
4. Houtkooper RH, Cantó C, Wanders RJ, Auwerx J (2010) The secret life of NAD^+: An old metabolite controlling new metabolic signaling pathways. *Endocr Rev* 31(2):194–223.
5. Lin SJ, Guarente L (2003) Nicotinamide adenine dinucleotide, a metabolic regulator of transcription, longevity and disease. *Curr Opin Cell Biol* 15(2):241–246.
6. Cantó C, et al. (2012) The NAD^+ precursor nicotinamide riboside enhances oxidative metabolism and protects against high-fat diet-induced obesity. *Cell Metab* 15(6): 838–847.
7. Houtkooper RH, Auwerx J (2012) Exploring the therapeutic space around NAD^+. *J Cell Biol* 199(2):205–209.
8. Mouchiroud L, et al. (2013) The NAD^+/sirtuin pathway modulates longevity through activation of mitochondrial UPR and FOXO signaling. *Cell* 154(2):430–441.
9. Oka S, Hsu CP, Sadoshima J (2012) Regulation of cell survival and death by pyridine nucleotides. *Circ Res* 111(5):611–627.
10. Pittelli M, et al. (2011) Pharmacological effects of exogenous NAD on mitochondrial bioenergetics, DNA repair, and apoptosis. *Mol Pharmacol* 80(6):1136–1146.
11. Wang S, et al. (2008) Cellular NAD replenishment confers marked neuroprotection against ischemic cell death: Role of enhanced DNA repair. *Stroke* 39(9):2587–2595.
12. Wiley C, Campisi J (2014) NAD^+ controls neural stem cell fate in the aging brain. *EMBO J* 33(12):1289–1291.
13. Chance B, Cohen P, Jobsis F, Schoener B (1962) Localized fluorometry of oxidation-reduction states of intracellular pyridine nucleotide in brain and kidney cortex of the anesthetized rat. *Science* 136(3513):325.
14. Lowry OH, Passonneau JV, Schulz DW, Rock MK (1961) The measurement of pyridine nucleotides by enzymatic cycling. *J Biol Chem* 236:2746–2755.
15. Lowry OH, Passonneau JV, Rock MK (1961) The stability of pyridine nucleotides. *J Biol Chem* 236:2756–2759.
16. Avi-Dor Y, Olson JM, Doherty MD, Kaplan NO (1962) Fluorescence of pyridine nucleotides in mitochondria. *J Biol Chem* 237(7):2377–2383.
17. Lu M, Zhu XH, Zhang Y, Chen W (2014) Intracellular redox state revealed by in vivo ^{31}P MRS measurement of NAD^+ and NADH contents in brains. *Magn Reson Med* 71(6): 1959–1972.
18. Evans FE, Kaplan NO (1977) ^{31}P nuclear magnetic resonance studies of HeLa cells. *Proc Natl Acad Sci USA* 74(11):4909–4913.
19. Lei H, Zhu XH, Zhang XL, Ugurbil K, Chen W (2003) In vivo ^{31}P magnetic resonance spectroscopy of human brain at 7 T: An initial experience. *Magn Reson Med* 49(2): 199–205.
20. Navon G, Ogawa S, Shulman RG, Yamane T (1977) High-resolution ^{31}P nuclear magnetic resonance studies of metabolism in aerobic Escherichia coli cells. *Proc Natl Acad Sci USA* 74(3):888–891.
21. Du F, et al. (2008) Tightly coupled brain activity and cerebral ATP metabolic rate. *Proc Natl Acad Sci USA* 105(17):6409–6414.
22. Siesjo BK (1978) *Brain Energy Metabolism* (John Wiley & Sons, New York).
23. Lu M, Chen W, Zhu XH (2014) Field dependence study of in vivo brain ^{31}P MRS up to 16.4 T. *NMR Biomed* 27(9):1135–1141.
24. Akitt JW (1983) *NMR and Chemistry: An Introduction to the Fourier Transform—Multinuclear Ear* (Chapman and Hall Ltd, London), 2nd Ed, pp 45–49.
25. Alano CC, et al. (2007) Differences among cell types in NAD^+ compartmentalization: A comparison of neurons, astrocytes, and cardiac myocytes. *J Neurosci Res* 85(15): 3378–3385.
26. McKenna MC, Waagepetersen HS, Schousboe A, Sonnewald U (2006) Neuronal and astrocytic shuttle mechanisms for cytosolic-mitochondrial transfer of reducing equivalents: Current evidence and pharmacological tools. *Biochem Pharmacol* 71(4):399–407.
27. Williamson DH, Lund P, Krebs HA (1967) The redox state of free nicotinamide-adenine dinucleotide in the cytoplasm and mitochondria of rat liver. *Biochem J* 103(2): 514–527.
28. Tischler ME, Friedrichs D, Coll K, Williamson JR (1977) Pyridine nucleotide distributions and enzyme mass action ratios in hepatocytes from fed and starved rats. *Arch Biochem Biophys* 184(1):222–236.
29. Balaban RS (1990) Regulation of oxidative phosphorylation in the mammalian cell. *Am J Physiol* 258(3 Pt 1):C377–C389.
30. Chance B (1976) Pyridine nucleotide as an indicator of the oxygen requirements for energy-linked functions of mitochondria. *Circ Res* 38(5 Suppl 1):I31–I38.
31. Vaishnavi SN, et al. (2010) Regional aerobic glycolysis in the human brain. *Proc Natl Acad Sci USA* 107(41):17757–17762.
32. Balaban RS, Nemoto S, Finkel T (2005) Mitochondria, oxidants, and aging. *Cell* 120(4): 483–495.
33. Stein LR, Imai S (2012) The dynamic regulation of NAD metabolism in mitochondria. *Trends Endocrinol Metab* 23(9):420–428.
34. Braidy N, et al. (2014) Mapping NAD^+ metabolism in the brain of ageing Wistar rats: Potential targets for influencing brain senescence. *Biogerontology* 15(2):177–198.
35. Gomes AP, et al. (2013) Declining NAD^+ induces a pseudohypoxic state disrupting nuclear-mitochondrial communication during aging. *Cell* 155(7):1624–1638.
36. Leenders KL, et al. (1990) Cerebral blood flow, blood volume and oxygen utilization. Normal values and effect of age. *Brain* 113(Pt 1):27–47.
37. Yamaguchi T, et al. (1986) Reduction in regional cerebral metabolic rate of oxygen during human aging. *Stroke* 17(6):1220–1228.
38. Navarro A, Boveris A (2007) The mitochondrial energy transduction system and the aging process. *Am J Physiol Cell Physiol* 292(2):C670–C686.
39. Boumezbeur F, et al. (2010) Altered brain mitochondrial metabolism in healthy aging as assessed by in vivo magnetic resonance spectroscopy. *J Cereb Blood Flow Metab* 30(1):211–221.
40. Petersen KF, et al. (2003) Mitochondrial dysfunction in the elderly: Possible role in insulin resistance. *Science* 300(5622):1140–1142.
41. Schreiber V, Dantzer F, Ame JC, de Murcia G (2006) Poly(ADP-ribose): Novel functions for an old molecule. *Nat Rev Mol Cell Biol* 7(7):517–528.
42. Wang J, et al. (2010) The role of Sirt1: At the crossroad between promotion of longevity and protection against Alzheimer's disease neuropathology. *Biochim Biophys Acta* 1804(8):1690–1694.
43. Yoshino J, Mills KF, Yoon MJ, Imai S (2011) Nicotinamide mononucleotide, a key NAD^+ intermediate, treats the pathophysiology of diet- and age-induced diabetes in mice. *Cell Metab* 14(4):528–536.
44. Mouchiroud L, Houtkooper RH, Auwerx J (2013) NAD^+ metabolism: A therapeutic target for age-related metabolic disease. *Crit Rev Biochem Mol Biol* 48(4):397–408.
45. Prolla TA, Denu JM (2014) NAD^+ deficiency in age-related mitochondrial dysfunction. *Cell Metab* 19(2):178–180.
46. Klingenberg M, Buecher T (1960) Biological oxidations. *Annu Rev Biochem* 29: 669–708.
47. Unden G, Bongaerts J (1997) Alternative respiratory pathways of Escherichia coli: Energetics and transcriptional regulation in response to electron acceptors. *Biochim Biophys Acta* 1320(3):217–234.